Electromagnetic production of Σ hypernuclei

C. Bennhold
Institut für Kernphysik, Johannes Gutenberg-Universität, 6500 Mainz, Federal Republic of Germany
(Received 4 October 1988)

The formation of sigmas through low-energy kaon photoproduction from nucleons is described by using Feynman diagrams. Different models for the production process are compared, including pseudovector versus pseudoscalar coupling for the $KN\Sigma$ vertex. The elementary coupling constants are fitted to the cross-section data up to 2.2 GeV and agree with previous fits obtained from the photoproduction of lambdas from protons. This operator is then implanted into the nucleus via the impulse approximation. Using Woods-Saxon shell-model wave functions for the sigma and the nucleon and a particle-hole basis for the nucleus, angular distributions are obtained for the formation of ${}^{16}_{\Sigma}$N, ${}^{40}_{\Sigma}$K, and ${}^{208}_{\Sigma}$Tl. Cross sections for processes employing the reaction ${}^1\mathrm{H}(\gamma,K^+)\Sigma^0$ are about one fifth of those corresponding to lambda hypernuclei, while reactions involving $n(\gamma,K^+)\Sigma^-$ yield counting rates comparable to those of lambda-hypernuclear photoproduction.

I. INTRODUCTION

New experimental facilities under construction or consideration in the multi-GeV regime have created an increased interest in the electro- and photoproduction of hypernuclei.[1-5] While the formation and excitation of Λ-hypernuclei with real as well as virtual photons along with the elementary production mechanism has been studied for several years, no estimates of Σ-hypernuclear photoproduction are available. This is partly due to the lack of information of the elementary process with far less cross section and no polarization data available as compared to Λ photoproduction.[6] Little is known about the Σ-nucleus potential,[7] which makes it difficult to obtain Σ-single-particle shell-model wave functions for a reliable nuclear calculation.

On the other hand, Σ hypernuclei have provided many puzzles over the last few years so that it seems reasonable to consider production mechanisms other than the usual (K^-,π) reaction[8] that has been employed to create Σ hypernuclei from the start in 1979. The well-known small widths of Σ peaks in the excitation function have been surprising not only because the Σ states produced up to now are unbound, but also they are expected to be short lived due to the strong $\Sigma N\rightarrow\Lambda N$ conversion process. Even though a recent version of the KEK data[9] with improved statistics indicates a broad structureless bump for ^{12}C, the question is not considered resolved. Σ-nuclear bound states have not been observed yet, and it is not clear if this is a consequence of the shallow Σ nuclear potential predicted by several models. Another open question concerns the magnitude of the Σ-nucleus spin-orbit splitting, where different analyses and models predict a ratio $R=V_{ls}^{\Sigma}/V_{ls}^{N}$ of 0.5 to 2.

This paper is a straightforward extension of previous work involving Λ photoproduction[5,6] and is similar to a recent study by Kadowaki and Suzuki.[10] The advantages of an electromagnetic production mechanism involving the weakly distorted K^+, as well as its ability to preferentially excite high-spin and unnatural parity states are well documented and will not be repeated here.

In Sec. II we develop different models for the elementary process ${}^1\mathrm{H}(\gamma,K^+)\Sigma^0$ and compare them with the available low-energy data. The nuclear calculation based on the impulse approximation is presented in Sec. III along with a variety of angular distributions for the hypernuclei ${}^{16}_{\Sigma}$N, ${}^{40}_{\Sigma}$K, and ${}^{208}_{\Sigma}$Tl. We summarize our findings in Sec. IV.

II. THE ELEMENTARY PROCESS

The basic ingredient to an analysis of Σ-hypernuclear photoproduction is an elementary photoproduction operator that can be used in the nuclear environment. For this purpose we choose Feynman diagrams to describe the elementary process, since this assures a frame independent operator which is needed to include Fermi motion in the nucleus. In this section we follow Refs. 6 and 11 in deriving the amplitudes for the reactions ${}^1\mathrm{H}(\gamma,K^+)\Sigma^0$ and $n(\gamma,K^+)\Sigma^-$. Even though data are only available for the former process, the latter one could be studied on the deuteron or heaver nuclei. Employing the formalism developed in Ref. 11, we write the basic matrix element in the notation of Bjorken and Drell[12] as

$$M_{fi}=\bar{u}(p_\Sigma)\sum_{j=1}^{4}A_j(s,t)M_j u(p_N)\ , \tag{1}$$

where the gauge and Lorentz invariant matrices are given by

$$\begin{aligned}
M_1&=-\gamma_5\not{\epsilon}\not{p}_\gamma\ ,\\
M_2&=2\gamma_5(\epsilon\cdot p_N p_\gamma\cdot p_\Sigma-\epsilon\cdot p_\Sigma p_\gamma\cdot p_N)\ ,\\
M_3&=\gamma_5(\not{\epsilon}p_\gamma\cdot p_N-\not{p}_\gamma\epsilon\cdot p_N)\ ,\\
M_4&=\gamma_5(\not{\epsilon}p_\gamma\cdot p_\Sigma-\not{p}_\gamma\epsilon\cdot p_\Sigma)\ ,
\end{aligned} \tag{2}$$

with $p_\gamma=(E_\gamma,\mathbf{p}_\gamma)$, p_N, p_K, and p_Σ being the four vectors of the photon, nucleon, kaon, and sigma, respectively.

The four amplitudes A_j depend only on the elementary coupling constants and the Mandelstam variables

$$s=(p_N+p_\gamma)^2,\quad t=(p_\gamma-p_K)^2,\quad u=(p_N-p_K)^2\ .$$

The basic diagrams are given by the nucleon exchange in the direct or s channel, kaon exchange in the t channel, and sigma exchange in the u channel. Usually included in the model are the exchange of a lambda in the u channel in case of Σ^0 photoproduction and the K^* in the t channel, which is a 1^- resonance of the kaon. The Born amplitudes for the N,K^+, and Σ exchange in pseudoscalar (PS) coupling are given by

$$\begin{aligned}
A_1^{\text{Born}}&=\frac{g_\Sigma e}{s-M_N^2}(q_N+\kappa_N)+\frac{g_\Sigma e}{u-M_\Sigma^2}(q_\Sigma+\kappa_\Sigma)\ ,\\
A_3^{\text{Born}}&=\frac{g_\Sigma e}{s-M_N^2}\frac{\kappa_N}{M_N}\ ,\\
A_4^{\text{Born}}&=\frac{g_\Sigma e}{u-M_\Sigma^2}\frac{\kappa_\Sigma}{M_\Sigma}\ ,\\
A_2^{\text{Born}}&=\frac{2eg_\Sigma}{(s-M_N^2)(t-M_K^2)},\quad \text{for } {}^1\text{H}(\gamma,K^+)\Sigma^0\ ,\\
A_2^{\text{Born}}&=-\frac{2eg_\Sigma}{(u-M_\Sigma^2)(t-M_K^2)},\quad \text{for } n(\gamma,K^+)\Sigma^-\ ,
\end{aligned}\tag{3}$$

with q_N,q_Σ and κ_N,κ_Σ denoting the charge and anormalous magnetic moments of the nucleon and hyperon, respectively, and $g_\Sigma=g_{K\Sigma N}$. In case of Σ^0 photoproduction there is a contribution from the Λ exchange to the amplitudes A_1 and A_4

$$A_1^\Lambda=\frac{G_\Lambda e}{u-M_\Lambda^2},\quad A_4^\Lambda=\frac{G_\Lambda e}{u-M_\Lambda^2}\frac{2}{M_\Lambda+M_\Sigma}\tag{4}$$

with $G_\Lambda=\kappa_T g_{K\Lambda N}$, where κ_T is the $\Lambda\Sigma$-transition moment. The amplitudes for the K^* and other resonances in the s and u channel can be found in Ref. 6. Performing the analysis in pseudovector (PV) theory requires an additional diagram, the contact or "seagull" term, and replacing the coupling at the $K\Sigma N$ vertex $i\gamma_5$ by $[\not{q}/(M_N+M_\Sigma)]\gamma_5$ with q being the exchanged four momentum. Only the amplitude A_1 has an additional contribution given by[13]

$$A_1^{\text{PV}}=A_1^{\text{PS}}+\frac{eg_\Sigma}{2(M_N+M_\Sigma)}\left[\frac{\kappa_N}{M_N}+\frac{\kappa_\Sigma}{M_\Sigma}\right]+\frac{eG_\Lambda}{(M_\Lambda+M_\Sigma)(M_\Lambda+M_N)}\ .\tag{5}$$

The magnetic moments of the proton and neutron are well known, whereas μ_{Σ^-} has been determined to be (-1.41 ± 0.25) nm. Since the magnetic moment of the Σ^0 has not been measured, we used the SU(3) relationship $\mu_{\Sigma^0}=-\frac{1}{2}\mu_N$, μ_N being the magnetic moment of the neutron.

Compared to the process ${}^1\text{H}(\gamma,K^+)\Lambda^0$, less cross-section and no polarization data are available for ${}^1\text{H}(\gamma,K^+)\Sigma^0$ in the low-energy regime from threshold [which is $E_{\text{lab}}^\gamma=1.046$ MeV for ${}^1\text{H}(\gamma,K^+)\Sigma^0$ and 1.052 MeV for $n(\gamma,K^+)\Sigma^-$] to about 2.2 GeV.[14] Since our primary goal is to provide an effective production operator suitable for nuclear calculations, we performed a least-squares fit to the available data in pseudoscalar and pseudovector theory for the Born terms (including the Λ and K^* exchange). The effective coupling constants obtained from this fit are presented in Table I, where we have defined $G_V=g_{K^*K\gamma}g^V_{K^*\Sigma N}$ and $G_T=g_{K^*K\gamma}g^T_{K^*\Sigma N}$, representing the vector and tensor coupling of the K^* at the $K^*\Sigma N$ vertex. Note that the reduced χ^2 is slightly better for PS-Born terms (row 1) as compared to PV-Born terms (row 2), which is reminiscent of the situation for Λ photoproduction.[15] The coupling constant $g_{K\Lambda N}$ can be obtained from G_Λ by dividing out the $\Lambda\Sigma$-transition moment to yield $g_{K\Lambda N}/\sqrt{4\pi}=2.15$ for the PS mode and 1.87 for the PV mode, which is to be compared with the respective values extracted from ${}^1\text{H}(\gamma,K^+)\Lambda$, namely 2.00 and 1.65 for PS and PV theory,[15] respectively. However, even though the values for $g_{K\Lambda N}$ are in agreement, $g_{K\Sigma N}$ varies widely in the different fits.

The χ^2 for the Born terms is rather large, indicating that resonant states in the direct and crossed channels should be included. However, little is known about the required parameters of the higher resonances, and the limited amount of data for Σ photoproduction would make a result obtained with too many adjustable parameters meaningless. We, therefore, allowed for only one resonance to contribute to the fit. As an obvious first choice we included the $\Delta(1236)$, known to be very important in pion-nuclear reactions, but, surprisingly, this reduced the χ^2 only slightly. Consequently, we included higher resonances up to spin $\frac{3}{2}$ and up to 2.2 GeV in the fit and found that the s channel $\Delta(1700)$ with spin $\frac{3}{2}^-$ was able to significantly improve the fit to the data. The preference of the data of the $\Delta(1700)$ over the $\Delta(1236)$ might be explained by its proximity to threshold ($E_{\text{total}}^{\text{c.m.}}=1685$ MeV), but the final conclusion will have to await further data. We do not claim theoretical rigor for our method; our goal is a reasonable description of the elementary data in terms of an effective operator in order to obtain a rough estimate of Σ hypernuclear cross sections. The resulting coupling constants and χ^2 are given in the third

TABLE I. Coupling constants obtained by a least-squares fit.

	$\frac{g_\Sigma}{\sqrt{4\pi}}$	$\frac{G_\Lambda}{\sqrt{4\pi}}$	$\frac{G_V}{4\pi}$	$\frac{G_T}{4\pi}$	$\frac{G_\Delta^1}{4\pi}$	$\frac{G_\Delta^2}{4\pi}$	χ^2
PS	2.20	−4.82	0.113	−0.038	0.0	0.0	5.60
PV	1.50	−4.20	0.068	−0.063	0.0	0.0	5.90
PS+delta	2.72	−3.60	0.104	0.005	−0.069	0.314	3.15

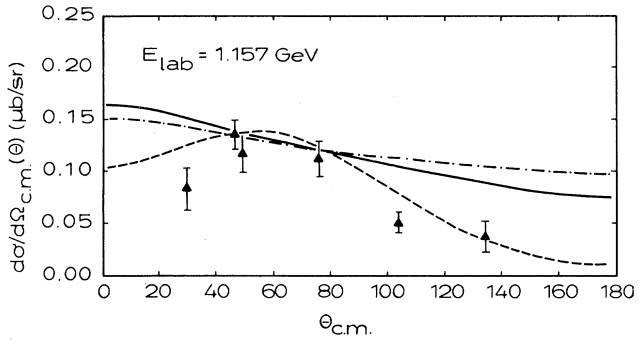

FIG. 1. Differential cross section for the process $^1H(\gamma,K^+)\Sigma^0$ in the cm system for $E^{\gamma}_{lab}=1157$ MeV with the solid curve showing PS-Born terms, the dashed-dotted curve PV-Born terms, and the dashed curve showing the PS-Born plus delta resonance terms.

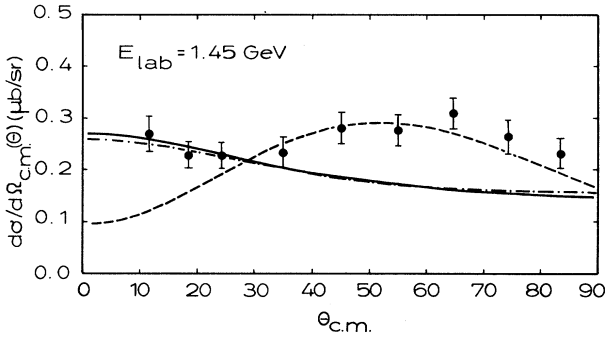

FIG. 2. As in Fig. 1 for $E^{\gamma}_{lab}=1450$ MeV.

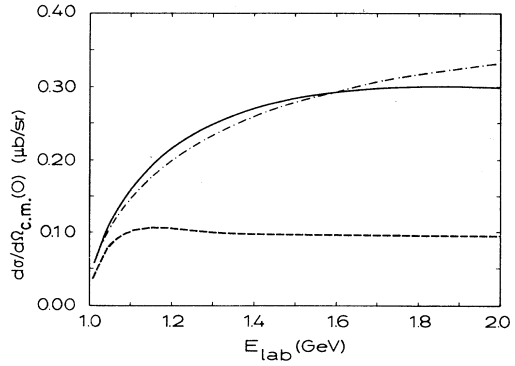

FIG. 3. Differential cross section at 0° as a function of photon lab energy. Everything else as in Fig. 1.

row of Table I, where G^1_Δ and G^2_Δ indicate the two possible electromagnetic couplings at the $\gamma\Delta N$ vertex. Note that the delta resonances could not contribute to Λ photoproduction due to isospin conservation.

Figures 1 and 2 illustrate the difference between the three models at a given photon laboratory energy. While there is little difference between PS and PV theory, including the $\Delta(1700)$ resonance improves the description of the data. In Fig. 3, one can see that the delta decreases the effect of the nonresonant background almost from threshold on. Clearly more data are needed to perform a reliable analysis and uniquely determine the influence of resonances on the elementary process.

III. Σ-HYPERNUCLEAR EXCITATION

Calculating nuclear matrix elements of the photoproduction operator in an impulse approximation framework requires knowledge of the single-particle wave function of a Σ bound in the nucleus. Contrary to the case of Λ hypernuclei,[16] not much strength has been observed below the Σ threshold in the Σ formation spectra from (K,π) reactions,[8] indicating a mean field that is considerably weaker for the Σ than for the Λ. Due to this lack of experimental information, we used a theoretical calculation done by Kohno,[17] who started from a microscopic density-dependent effective ΣN interaction[18] and obtained an Σ-single-particle potential as a Hartree insertion over occupied nucleon hole states. The resulting shallow Σ potential yields no bound states for ^{12}C and a barely bound Os state for the $A=17$ system, which seems consistent with observed Σ^--formation spectra from $(K^-\pi^+)$ reactions.[19] We parametrized the Σ potentials obtained by Kohno using the usual Woods-Saxon form and adjusted the depth and radial parameters to reproduce his single-particle energies and rms radii.

The resulting parameters for the $A=16$, 40, and 208 systems are given in Table II, where the diffuseness is given by a, and the radius is $R=r_0(A-1)^{1/3}$. Due to the peculiar behavior of the Σ potential as discussed in Ref. 17, the parameters vary widely for the three different nuclear systems. Since various analyses predict the ratio of Σ to N-nucleus spin-orbit potential $R=V^{\Sigma}_{ls}/V^{N}_{ls}$ to be between 0.5 and 2, we simply neglect the Σ spin-orbit interactions in our calculations below. Separation energies for the Σ^0 and Σ^- are listed in Table III, where we have included an additional attractive Coulomb potential that brings about single-particle energy shifts reminiscent of those between protons and neutrons. The nucleon bound-state wave functions used in our calculations are obtained by solving the Schrödinger equation with standard central and spin-orbit potentials of Woods-Saxon

TABLE II. Parameters for the Σ potential.

	$^{16}_{\Sigma}N$	$^{40}_{\Sigma}K$	$^{208}_{\Sigma}Tl$
r_0 (fm)	1.25	0.8	1.0
a (fm)	0.6	0.5	0.6
V_{cen} (MeV)	6	24	28

TABLE III. Σ-single-particle separation energies (in MeV).

	$^{16}_{\Sigma}$N		$^{40}_{\Sigma}$K		$^{208}_{\Sigma}$Tl	
	Σ^0	Σ^-	Σ^0	Σ^-	Σ^0	Σ^-
0*s*	~0	3.4	9.7	20.5	23.4	49.0
0*p*			~0	9.1	18.9	43.4
0*d*				2.3	13.7	37.2
1*s*					12.2	36.1
0*f*					7.5	30.5
1*p*					5.9	28.9
0*g*					1.8	23.4
1*d*						21.6

shape, where parameters have been adjusted to fit binding energies and rms radii.[20]

To invoke the impulse approximation we separate the nuclear structure aspects from the single-particle matrix elements by writing the many-body matrix elements as

$$\langle J_f M_f; K^+|T|J_i M_i;\gamma\rangle = \sum_{\alpha\alpha'} \langle J_f M_f|b^+_{\alpha'}a_\alpha|J_i M_i'\rangle\langle\alpha';K^+|t|\alpha;\gamma\rangle \ , \quad (6)$$

where we have assumed t to be a one-body operator. For simplicity we choose a pure particle-hole configuration for the nucleus, which eliminates the sum over the single-particle states α and α' in Eq. (6). Using distorted waves for the kaons we can write the matrix elements in coordinate space

$$\langle\alpha';K^+|t|\alpha;\gamma\rangle = \int d^3r\, \Psi^*_{\alpha'}(\mathbf{r})\Phi_K^{*(-)}(\mathbf{r})t(\mathbf{Q})e^{i\mathbf{k}\cdot\mathbf{r}}\Psi_\alpha(\mathbf{r}) \ , \quad (7)$$

where $\mathbf{Q}$ is the momentum transfer to the nucleus and $\Phi_K^{(-)}$ fulfills the boundary conditions of an outgoing kaon. A first-order optical potential[21] has been used to describe K^+ distortion with parameters obtained from a K^+N phase shift analysis.[22]

The elementary production operator can be divided into a spin-1 and spin-0 transition amplitude

$$t = L + i\boldsymbol{\sigma}\cdot\mathbf{K} = \sum_{s,m_s} i^s(-1)^{m_s}\sigma^s_{-m_s}K^s_{m_s} \ , \quad (8)$$

where $\sigma^0=1$ and $K^0_0=L$. To arrive at a cross section we carry out the spin projection summations to obtain

$$\sum_{M_i M_f} |\langle J_f M_f;K^+|T|J_i M_i;\gamma\rangle|^2 = \sum_{J,M}|F^J_M|^2 \ , \quad (9)$$

where F^J_M is given in the LS-coupling scheme

$$F^J_M = 4\pi\hat{J}\hat{j}' \sum_{\substack{L,S\\ l_\gamma,l_K}} i^{S+l_\gamma+l_K}(-1)^{l_K+L+S}\hat{L}\hat{S}\hat{l}_\gamma\hat{l}_K\hat{l}'\hat{l} \begin{bmatrix} l_\gamma & l_K & L\\ 0 & 0 & 0\end{bmatrix}\begin{bmatrix} l' & l & L\\ 0 & 0 & 0\end{bmatrix}\begin{Bmatrix} l' & \frac{1}{2} & j'\\ l & \frac{1}{2} & j\\ L & S & J\end{Bmatrix}$$
$$\times\{[Y_{l_\gamma}(\hat{\mathbf{k}})\times Y_{l_K}(\hat{\mathbf{q}})]^L\times K^S\}^J_M\int r^2\,dr\,\rho(r)U_{l_K,q}(r)j_{l_\gamma}(kr) \ , \quad (10)$$

where $\rho(r)=\psi_{n'l'j'}(r)\cdot\psi_{nlj}(r)$ is the product of the sigma and nucleon bound-state wave functions, $U_{l_K,q}(r)$ is the radial wave function of the distorted kaon with asymptotic momentum $\mathbf{q}$ and orbital angular momentum l_K, and the operator K^S is evaluated for frozen nucleons. Details of the calculation are presented elsewhere.[20]

The nonrelativistic production operator has been obtained by reducing Eq. (1) to Pauli spin space. Dropping terms of order p^2/M^2 from products of the small spinor components we obtain for L and $\mathbf{K}$

$$L = \frac{G_1}{2k}\left[\frac{1}{M_N}\mathbf{p}(\boldsymbol{\epsilon}\times\mathbf{k}) - \frac{1}{M_\Sigma}\mathbf{p}'(\boldsymbol{\epsilon}\times\mathbf{k})\right] \quad (11)$$

$$\mathbf{K} = -\boldsymbol{\epsilon}\left[G_3 - G_1 + \frac{G_1}{2k}\left(\frac{\mathbf{k}\cdot\mathbf{p}}{M_N}+\frac{\mathbf{k}\cdot\mathbf{p}'}{M_\Sigma}\right)\right] + \mathbf{k}\left[\frac{G_1}{2k}\left(\frac{\boldsymbol{\epsilon}\cdot\mathbf{p}}{M_N}+\frac{\boldsymbol{\epsilon}\cdot\mathbf{p}'}{M_\Sigma}\right) - G_4\right] - \mathbf{p}\left[\frac{G_1 - kG_4}{2M_N}\right] + \mathbf{p}'\left[\frac{G_2+kG_4}{2M_\Sigma}\right]$$

where the four momenta of the nucleon, sigma, and photon are $p=(E,\mathbf{p})$, $\mathbf{p}'=(E',\mathbf{p}')$, and $k=(k,\mathbf{k})$, respectively, and we have chosen the usual gauge in the lab system of $\epsilon_0=0$, $\epsilon\cdot\mathbf{k}=0$. The G_i are defined in terms of the amplitudes A_i from Eq. (3)–(5) by

$$G_1=kA_1,\quad G_2=2A_2(\epsilon\cdot\mathbf{p}'k\cdot p-\epsilon\cdot\mathbf{p}k\cdot p'),$$
$$G_3=A_3k\cdot p+A_4k\cdot p',\quad G_4=A_3\epsilon\cdot\mathbf{p}+A_4\epsilon\cdot\mathbf{p}'. \tag{12}$$

In the following we have used the coupling constants for Born terms with PS coupling. PV theory yields almost identical results, whereas including the $\Delta(1700)$ slightly enhances the cross section but does not change the shape of the curves.

In Fig. 4 we show angular distributions of various transitions of the reaction $^{16}\mathrm{O}(\gamma,K^+)^{16}_{\Sigma}\mathrm{N}$. Since the Σ^0 is barely bound in the $A=16$ system, we have employed the process $n(\gamma,K^+)\Sigma^-$ to produce the final Σ hypernucleus $^{16}_{\Sigma^-}$N. Assuming isospin to be a good quantum number, the operator from Sec. II was used with a coupling constant $g_{\Sigma^-K^+n}=\sqrt{2}g_{\Sigma^0K^+p}$,[23] and lambda exchange in the u channel cannot contribute to this reaction.

Figure 4 shows one of the ground states of $^{16}_{\Sigma^-}$N, the $(s_{1/2},p^{-1}_{1/2})0^-$ state, which is zero at $\Theta_K=0°$ and has a maximum at about 5°. Also presented are the first excited states 1^- and 2^- with a $(s_{1/2},p^{-1}_{3/2})$ configuration, which are degenerate in the extreme particle-hole model. Realistically, one would expect the two levels to split by about a few hundred keV, depending on the strength for the residual ΣN interaction. As in previous studies on Λ hypernuclei, the 2^- state has the highest counting rates.

In Fig. 5 differential cross sections are shown for the production of the Σ^0, as well as the Σ^- in the reaction $^{40}\mathrm{C}(\gamma,K^+)^{40}_{\Sigma}\mathrm{K}$. Compared to the photoproduction of Λ hypernuclei, the cross section for Σ^0 production on ^{40}C is

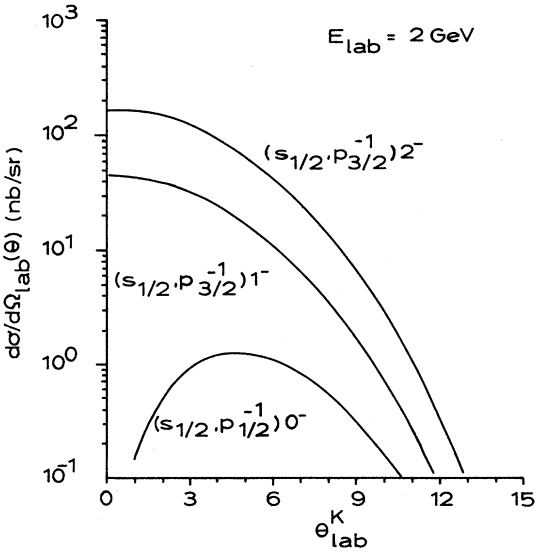

FIG. 4. Angular distributions in the lab system at $E^{\gamma}_{lab}=2$ GeV for the reaction $^{16}\mathrm{O}(\gamma,\mathrm{K}^+)^{16}_{\Sigma^-}\mathrm{N}$ for various transitions.

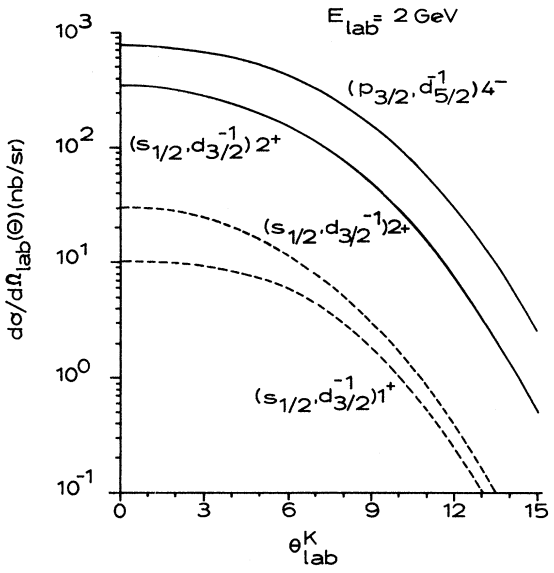

FIG. 5. Angular distributions for the reaction $^{40}\mathrm{C}(\gamma,K^+)^{40}_{\Sigma}\mathrm{K}$ where the solid (dashed) curves show transitions employing the mechanism $\gamma+n\rightarrow K^++\Sigma^-$ ($\gamma+p\rightarrow K^++\Sigma^0$).

lower by almost an order of magnitude; this is due to the momentum transfer being increased by $\Delta M=M_{\Sigma}-M_{\Lambda}\approx 80$ MeV. The 1^+ and 2^+ ground states of $^{40}_{\Sigma^0}$K are presented in Fig. 5; both states are falling off smoothly, with the 2^+ state having the higher cross section. The same 2^+ ground state is shown for Σ^- production with a cross section comparable to those of Λ photoproduction. Large cross sections are obtained for the $(p_{3/2},d^{-1}_{5/2})4^-$, almost reaching 1 μb for small kaon angles. This can be traced to the elementary process $n(\gamma,K^+)\Sigma^-$, which in this energy region yields cross sections five times higher than those of $^1\mathrm{H}(\gamma,K^+)\Sigma^0$. Kaon distortion is uniformly reducing the angular distributions by about a factor of 2 for the $A=40$ system.

Finally, Fig. 6 shows various high-spin excitations in the reaction $^{208}\mathrm{Pb}(\gamma,K^+)^{208}_{\Sigma}\mathrm{Tl}$, again employing the two different production mechanisms. The highest spin state, a $(g_{9/2},g^{-1}_{9/2})9^+$ substitutional transition has the highest counting rates and is almost constant up to $\Theta_K\approx 8°$ before falling off. Note that the next transition, a $(s_{1/2},i^{-1}_{13/2})7^+$ state still has a considerable cross section, even though the overlap integral between a $s_{1/2}$ and $i_{13/2}$ wave function is small. Similar in nature, but smaller in cross section, is the 6^- transition involving the Σ^0. Note that at higher angles kaon distortion fills in the minima for all three transitions. For comparison we present the 6^- transition calculated with plane waves and distorted waves. At small angles the cross section is suppressed by almost a factor of 5 due to distortion, while the cross section is clearly enhanced by orders of magnitude for large kaon angles.

In order to assess the influence of the Σ-hypernuclear spin-orbit coupling, we performed several calculations varying the spin-orbit potential between zero and twice

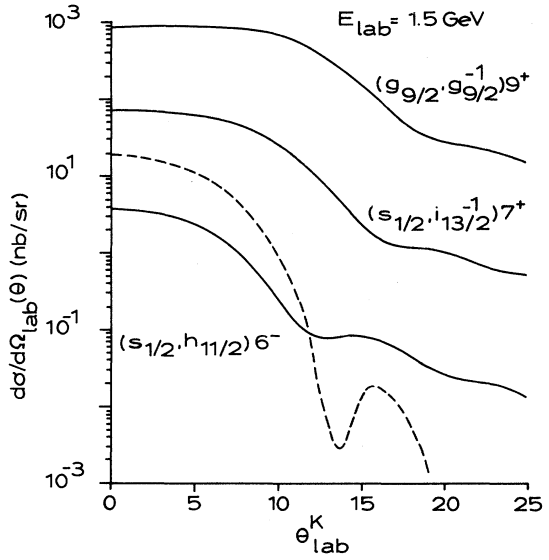

FIG. 6. Angular distributions for the reaction ^{208}Pb$(\gamma,K^+)^{208}_{\Sigma}$Tl at $E\gamma_{lab}=1.5$ GeV where the 9^+ and 7^+ transitions were calculated using $\gamma+n\rightarrow K^++\Sigma^-$ while the 6^- transition was evaluated using $\gamma+n\rightarrow K^++\Sigma^0$. The solid curves include distortion while the dashed curve has been calculated with plane waves.

the nuclear value, but found that the cross sections changed only up to 15%. It is therefore justified to neglect it at the present stage.

In general, the angular distributions shown in Figs. 4–6 are very similar to those of Λ-hypernuclear photoproduction.[1–5,20] Due to the rapidly increasing momentum transfer at $E\gamma_{lab}=2$ GeV, the cross section falls off by several orders of magnitude for $\Theta_K=0°-15°$. High-spin and unnatural parity states are preferentially excited.

IV. CONCLUSIONS

We have obtained an operator for the process ^{1}H$(\gamma,K^+)\Sigma^0$ based on diagrammatic techniques, whose coupling constants were fitted to cross section data up to 2.2 GeV. Using Born terms as well as an additional Λ and K^* exchange yields a satisfactory fit for PS and PV theory; however, the coupling constants differ by 30–40 %. The influence of resonances is uncertain due to the limited amount of data, even though the inclusion of the Δ(1700) in the s channel does improve the χ^2.

This photoproduction amplitude was then implanted into the nucleus in an impulse approximation framework. As expected, the angular distributions for the three reactions studied are very similar to those of Λ-hypernuclear photoproduction. Kaon distortion is not significant for light nuclear systems; however, for heavy nuclei the cross sections are enhanced at large kaon angles, improving the chances of performing exotic reactions that envision deeply bound hyperons in an environment close to nuclear matter. Since the operator K^s of Eq. (11) has been evaluated at a fixed initial nucleon momentum **p**, nonlocal effects arising from the propagation of the various hadrons have been neglected, but will be examined in the future.

The counting rates for Σ^- production are comparable to those of Λ-hypernuclear production, while those for Σ^0 photoproduction are smaller by a factor of 5 or more. Around 2 GeV such experiments should therefore be feasible at laboratories like the Continuous Electron Beam Accelerator Facility (CEBAF). Thus, kaon photoproduction may become another tool to shed some light on the problems of Σ-hypernuclear physics.

ACKNOWLEDGMENTS

I am grateful to M. Kohno for helpful discussions. This work was supported by the Deutsche Forschungsgemeinschaft (SFB 201).

[1] A. M. Bernstein, T. W. Donnelley, and G. N. Epstein, Nucl. Phys. **A358**, 195 (1981).
[2] S. S. Hsiao and S. R. Cotanch, Phys. Rev. C **28**, 1668 (1983); S. R. Cotanch and S. S. Hsiao, Nucl. Phys. **A450**, 195 (1986).
[3] J. Cohen, Phys. Rev. C **32**, 543 (1985); Proceedings of the Continuous Electron Beam Accelerator Facility (CEBAF) Summer workshop, 1986 (CEBAF, Newport News, VA, 1987), p. 305.
[4] A. S. Rosenthal, D. Halderson, and F. Tabakin, Phys. Lett. B **182**, 143 (1986); A. S. Rosenthal *et al.*, Ann. Phys. (N.Y.) **189**, 33 (1988).
[5] C. Bennhold and L. E. Wright, Phys. Lett. B **191**, 11 (1987); Prog. Part. Nucl. Phys. **20**, 377 (1988); *Proceedings of the 5th International Miniconference at National Instituut voor Kernphysica en Hoge-EnergieFysica (NIKHEF), Amsterdam, 1987* (NIKHEF, Amsterdam, 1987), p. 267.
[6] R. A. Adelseck, C. Bennhold, and L. E. Wright, Phys. Rev. C **32**, 1681 (1985).
[7] R. Wünsch and J. Zofka, Report UJF 86-11.
[8] R. Bertini *et al.*, Phys. Lett. **90B**, 375 (1980); **136B**, 29 (1984); **158B**, 19 (1985).
[9] R. S. Hayano *et al.*, *Proceedings of the 1986 Institute for Nuclear Study International Symposium on Hypernuclear Physics* (INS, University of Tokyo, Tokyo, 1986), p. 19.
[10] H. Kadowaki and Y. Suzuki, Prog. Theor. Phys. **79**, 263 (1988).
[11] G. F. Chew, M. L. Goldberger, F. B. Low, and Y. Nambu, Phys. Rev. **106**, 1337 (1957); **106**, 1345 (1957).
[12] J. D. Bjorken and S. D. Drell, *Relativistic Quantum Mechanics* (McGraw-Hill, New York, 1964).
[13] J. Cohen, Phys. Rev. C **37**, 187 (1988).
[14] H. Gööing *et al.*, Nucl. Phys. **B26**, 121 (1971); P. Feller *et al.*, Nucl. Phys. **B39**, 413 (1972); A. Bleckmann *et al.*, Z. Phys. **239**, 1 (1970); R. L. Anderson *et al.*, Phys. Rev. Lett. **9**, 1 (1962); T. Fujii *et al.*, Phys. Rev. D **2**, 439 (1970).
[15] C. Bennhold and L. E. Wright, Phys. Rev. C **36**, 438 (1987).

[16]W. Brückner *et al.*, Phys. Lett. **79B**, 157 (1978); C. Milner *et al.*, *ibid.* **54**, 1237 (1985).
[17]M. Kohno, Prog. Theor. Phys. **78**, 123 (1987).
[18]Y. Yamamoto and H. Bando, Prog. Theor. Phys. Suppl. **81**, 9 (1985).
[19]M. Kohno *et al.*, Nucl. Phys. **A470**, 609 (1987).
[20]C. Bennhold and L. E. Wright, Phys. Rev. C **39**, 927 (1989).
[21]C. B. Dover and G. E. Walker, Phys. Rep. **85**, 1 (1982).
[22]B. R. Martin, Nucl. Phys. **B94**, 413 (1975).
[23]O. Dumbrajs *et al.*, Nucl. Phys. **B216**, 277 (1983).